Time-domain modeling and computation for waves in some complex mediums

Liwei Xu

University of Electronic Science and Technology of China

Modeling and simulation of interface dynamics in fluids/solids and their applications
The institute for mathematical sciences, NUS

- Supported by NSFC (91630205, 11771068)

Outline

- Water waves on a liquid surface (Green-Naghdi equations)
- Elastic waves in solids
  - Elastic waves in homogeneous medium (acoustic-elastic or fluid-solid interactions)
  - Elastic waves in porous medium (Biot-Johnson-Koplic-Dashen equations)
- Electromagnetic waves in fluids
  - Compressible magnetohydrodynamic (MHD) equations
  - Incompressible magnetohydrodynamic (MHD) equations
  - Cold Plasma equations
- Development of central Discontinuous Galerkin schemes

Water wave eqations

- Full Euler equation: Let $\varphi(x,z,t)$ be the velocity potential satisfying

$$\Delta\varphi = 0 \quad \text{in} \quad S_\eta,$$

where $S_\eta = \{(x,z) \in \mathbb{R}^3 | -h + b(x) \le z \le \eta(x,t), x = (x_1, x_2) \in \mathbb{R}^2,\ t \ge 0\}$, with

$$\begin{aligned}
\partial_z\varphi &= 0 \quad \text{on} \quad z = -h + b(x)\ , \\
\partial_t\eta + \nabla_x\eta\cdot\nabla_x\varphi - \partial_z\varphi &= 0 \quad \text{on} \quad z = \eta(x,t)\ , \\
\partial_t\varphi + |\nabla\varphi|^2/2 + g\eta &= 0 \quad \text{on} \quad z = \eta(x,t)\ .
\end{aligned}$$

- Full nonlinearity and full dispersion

Runup of solitary waves with large amplitude

Example: Runup of solitary waves with large amplitude

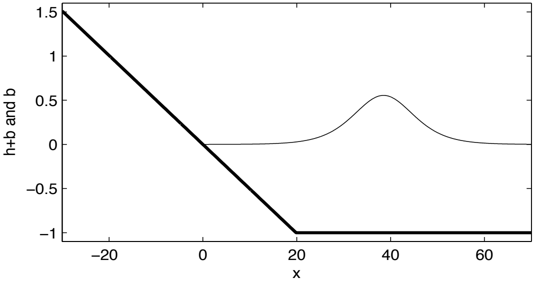

Figure: Initial solitary wave for the runup.

Runup of solitary waves with large amplitude

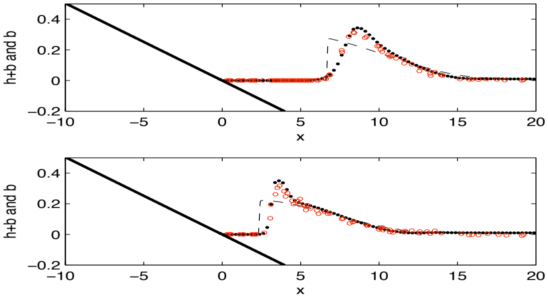

Figure: Runup of solitary wave with the amplitude $\eta = 0.28$ at $t = 15, 20$, (from top to bottom). Red circle: experimental data; black dashed line: nonlinear shallow water equations; black dots: Green-Naghdi model.

Harmonic generation over a submerged bar

Example: We now examine the propagation of Stokes waves over a submerged bar, the bottom variation is

$$b(x) = \begin{cases} -0.4 + 0.05(x-6) & \textit{for} \ \ 6 \le x \le 12, \\ -0.1 & \textit{for} \ \ 12 \le x \le 14, \\ -0.1 - 0.1(x-14) & \textit{for} \ \ 14 \le x \le 17, \\ -0.4 & \textit{elsewhere}. \end{cases}$$

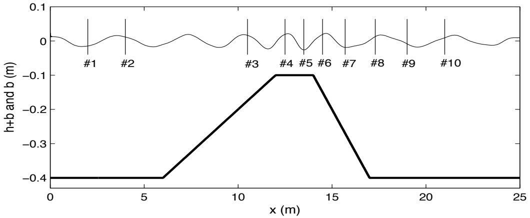

Figure: Experimental set-up and locations of the wave gauges.

Harmonic generation over a submerged bar

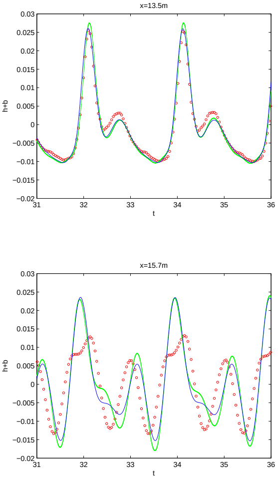

Figure: Time series of surface elevations for waves passing over a submerged bar. Red circles: experimental data, green solid line: CDG-FE method, blue solid line: PS-FE method.

Green-Naghdi equations

The Green-Naghdi equations read (Su-Garder 1969, Green-Naghdi 1976, Alvarez-Samaniego-Lannes 2008)

$$\begin{cases} h_t + (hu)_x + (hv)_y = 0, \\ (hu)_t + \left(hu^2 + \frac{1}{2}gh^2 + \frac{1}{3}h^3\Phi + \frac{1}{2}h^2\Psi\right)_x + (huv)_y = -\left(gh + \frac{1}{2}h^2\Phi + h\Psi\right) b_x, \\ (hv)_t + (huv)_x + \left(hv^2 + \frac{1}{2}gh^2 + \frac{1}{3}h^3\Phi + \frac{1}{2}h^2\Psi\right)_y = -\left(gh + \frac{1}{2}h^2\Phi + h\Psi\right) b_y. \end{cases} \tag{1}$$

where

$$\Phi = -u_{xt} - uu_{xx} + u_x^2 - v_{yt} - vv_{yy} + v_y^2 - uv_{xy} - u_{xy}v + 2u_x v_y, \tag{2}$$

$$\Psi = b_x u_t + b_x uu_x + b_{xx}u^2 + b_y v_t + b_y vv_y + b_{yy}v^2 + b_y uv_x + b_x u_y v + 2b_{xy}uv. \tag{3}$$

Green-Naghdi equations

From the second and third equations in (1), we have

$$\begin{aligned} u_t &= -g(h+b)_x - uu_x - u_y v + \text{higher order terms} \\ &\simeq \alpha u_t + (1-\alpha)(-g(h+b)_x - uu_x - u_y v), \end{aligned}$$

and

$$\begin{aligned} v_t &= -g(h+b)_y - vv_y - uv_x + \text{higher order terms} \\ &\simeq \alpha v_t + (1-\alpha)(-g(h+b)_y - vv_y - uv_x). \end{aligned}$$

Improved GN equations (X. et al., 2018)

Replacing u_t and v_t by $\alpha u_t + (\alpha-1)(uu_x + u_y v + g(h+b)_x)$ and $\alpha v_t + (\alpha-1)(vv_y + uv_x + g(h+b)_y)$ in (2) and (3), respectively, yields

$$\begin{cases} h_t + (hu)_x + (hv)_y = 0, \\ (hu)_t + \left(hu^2 + \frac{1}{2}gh^2 + \frac{1}{3}h^3\Phi + \frac{1}{2}h^2\Psi\right)_x + (huv)_y = -\left(gh + \frac{1}{2}h^2\Phi + h\Psi\right) b_x, \\ (hv)_t + (huv)_x + \left(hv^2 + \frac{1}{2}gh^2 + \frac{1}{3}h^3\Phi + \frac{1}{2}h^2\Psi\right)_y = -\left(gh + \frac{1}{2}h^2\Phi + h\Psi\right) b_y. \end{cases} \tag{4}$$

with

$$\begin{aligned} \Phi &= -\alpha u_{tx} - (\alpha-2)u_x^2 - \alpha uu_{xx} - \alpha u_{xy}v - 2(\alpha-1)u_y v_x - (\alpha-1)g(h+b)_{xx} \\ &\quad -\alpha v_{ty} - (\alpha-2)v_y^2 - \alpha vv_{yy} - \alpha uv_{xy} - (\alpha-1)g(h+b)_{yy} + 2u_x v_y, \qquad (5) \\ \Psi &= \alpha b_x u_t + \alpha b_x uu_x + \alpha b_x u_y v + (\alpha-1)gb_x(h+b)_x + \alpha b_y v_t \\ &\quad +\alpha b_y vv_y + \alpha b_y uv_x + (\alpha-1)gb_y(h+b)_y + b_{xx}u^2 + b_{yy}v^2 + 2b_{xy}uv. \qquad (6) \end{aligned}$$

It is obvious that the Green-Naghdi model (1) corresponds to a particular case of the Green-Naghdi model (4) with $\alpha = 1.0$.

Dispersion effect comparison (X. et al., 2018)

We compare the linear dispersion relation of the Green-Naghdi equations and that of the full water wave problem in finite depth,

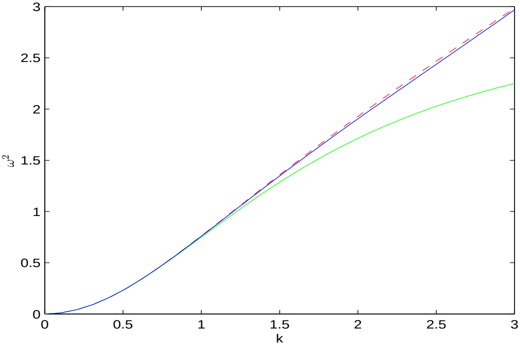

Figure: Comparison between the linear dispersion relation of the Green-Naghdi equations with $\alpha = 1.0$ (green solid line) and $\alpha = 1.159$ (blue solid line) and the exact linear dispersion relation of the full water wave problem (red dashed line), with $g = 1$, $h_0 = 1$ and $u_0 = 0$.

Challenges (X. et al., JCP (2014), SISC (2016), JSC(2017), 2018)

- Modeling
  - High nonlinearity (full)
  - Strong dispersion
- Computation
  - Remove the mixed time and space derivatives
  - Balance the flux term and the source term

$$u = 0 \,, \qquad h + b = \text{constant} \,,$$

  - Maintain the non-negativity of the water depth

Numerical results

Example: Harmonic generation over a submerged bar. This example exhibits the propagation of Stokes waves over a submerged bar in Figure 6 in which we also label the positions of 10 gauges. At initial time, $h + b = 0$ and $u = 0$ in the computational domain. The incident wave (entering from the left) is a third-order Stokes wave. An outgoing condition is applied at the right boundary.

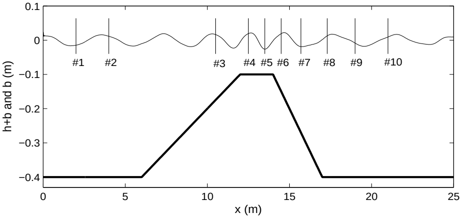

Figure: Experimental set-up and locations of the wave gauges.

Numerical results

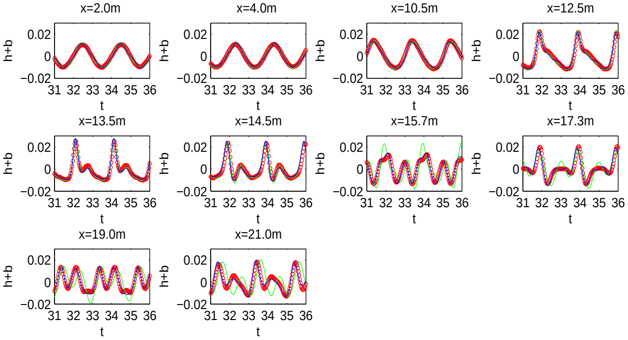

Figure: Time series of surface elevations for waves passing over a submerged bar. Circles: experimental data, green solid line: numerical results with $\alpha = 1$, blue solid line: numerical results with $\alpha = 1.159$.

Introduction

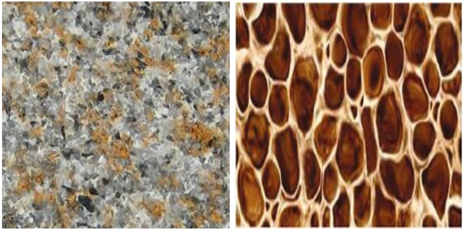

(a) **(b)**

Figure: (a) Close-up view of sandstone, (b) bone with osteoporosis.

Wave propagation in poroelastic media is described by Biot's theory and Johnson-Koplik-Dashen dynamic permeability model.

- M. A. Biot, J. Acoust. Soc. Amer., 28(1956).
- M. A. Biot, J. Acoust. Soc. Amer., 28(1956).
- D.L. Johnson, J. Koplik, R. Dashen. J. Fluid Mech., 176(1987).

Mathematical models

多孔介质中的波动现象可以用多孔弹性理论来描述，Biot理论指出多孔介质中有三个波：Fast P wave, S wave, Slow P wave。定义特征频率为$f_c := min_{i=x,y,z}(\frac{\phi\eta}{T_i k_i \rho_f})$，当频率小于$f_c$ 时用Biot模型来描述，当频率大于f_c时用Johnson-Koplik-Dashen(JDK)模型来描述，相应的数学方程可以表示为：

$$\partial_t \mathbf{Q} + \nabla \cdot \mathbf{F}(\mathbf{Q}) = \mathbf{h}(\mathbf{Q}) + (\mathbf{S}) \tag{7}$$

其中$\mathbf{Q} = (\tau_{xx}\ \tau_{zz}\ \tau_{xz}\ v_x\ v_z\ p\ q_x\ q_z)^\top$ 是未知向量, τ是应力，p是压力，$\mathbf{v}$ 是固体质点速度，$\mathbf{q}$ 是相对速度，$\mathbf{F} = (\mathbf{f}, \mathbf{g})$是通量函数，$\mathbf{h}$ 是粘性项，$\mathbf{S}$ 是外加的源项。相应的表达式为：

$$\begin{aligned}
\mathbf{f}(\mathbf{Q}) = &-(c_{11}^u v_x + \alpha_1 M q_x, c_{13}^u v_x + \alpha_3 M q_x, c_{55}^u v_z, \frac{m_1}{\Delta_1}\tau_{xx} + \frac{\rho_f}{\Delta_1}p, \frac{m_3}{\Delta_3}\tau_{xz}, \\
&-\alpha_1 M v_x - M q_x, -\frac{\rho_f}{\Delta_1}\tau_{xx} - \frac{\rho}{\Delta_1}p, -\frac{\rho_f}{\Delta_3}\tau_{xz})^\top, \\
\mathbf{g}(\mathbf{Q}) = &-(c_{13}^u v_z + \alpha_1 M q_z, c_{33}^u v_z + \alpha_3 M q_z, c_{55}^u v_x, \frac{m_1}{\Delta_1}\tau_{xz}, \frac{m_3}{\Delta_3}\tau_{zz} + \frac{\rho_f}{\Delta_3}p, \\
&-\alpha_3 M v_z - M q_z, -\frac{\rho_f}{\Delta_1}\tau_{xz}, -\frac{\rho_f}{\Delta_3}\tau_{zz} - \frac{\rho}{\Delta_3}p)^\top.
\end{aligned} \tag{8}$$

Mathematical models

在低频的时候，粘性项为：

$$\mathbf{h}_{\mathbf{low}}(\mathbf{Q}) = \left(0,0,0,\frac{\rho_f\eta}{\Delta_1 k_1}q_x,\frac{\rho_f\eta}{\Delta_3 k_3}q_z,0,-\frac{\rho\eta}{\Delta_1 k_1}q_x,-\frac{\rho\eta}{\Delta_3 k_3}q_z\right)^\top, \tag{9}$$

高频时候，粘性项为：

$$\begin{aligned}\mathbf{h}_{\mathbf{high}}(\mathbf{Q}) =&\Big(0,0,0,\frac{\rho_f\eta}{\Delta_1 k_1\sqrt{\Omega_1}}(D+\Omega_1)^{1/2}q_x,\frac{\rho_f\eta}{\Delta_3 k_3\sqrt{\Omega_3}}(D+\Omega_3)^{1/2}q_z,\\ &0,-\frac{\rho\eta}{\Delta_1 k_1\sqrt{\Omega_1}}(D+\Omega_1)^{1/2}q_x,-\frac{\rho\eta}{\Delta_3 k_3\sqrt{\Omega_3}}(D+\Omega_3)^{1/2}q_z\Big)^\top.\end{aligned} \tag{10}$$

其中的参数为：porosity $0 \le \phi \le 1$, density ρ_f, ρ_s and $\rho = (1-\phi)\rho_s + \phi\rho_f$, viscousity η, the fluid bulk modulus K_f, the solid bulk modulus K_s, tortuosities $T_{x,z} \ge 1$, permeability $k_{x,z}$, the viscous characteristic length $\Lambda_{x,z}$, the Pride number $P_i = \frac{4T_ik_i}{\phi\Lambda_i^2}$, $i = x,z$, the undrained elastic constants $c_{ij}^u = c_{ij}^{(m)} + M\alpha_i\alpha_j$, $i,j = 1,...5$, $c_{66}^u = \frac{1}{2}(c_{11}^u - c_{12}^u)$, $\alpha_1 = 1 - \frac{c_{11}^{(m)}+c_{12}^{(m)}+c_{12}^{(m)}}{3K_s}$, $\alpha_2 = \alpha_1$, $\alpha_3 = 1 - \frac{2c_{13}^{(m)}+c_{33}^{(m)}}{3K_s}$, $\alpha_{4,5,6} = 0$, $M = \frac{K_s^2}{K_s[1+\phi(K_s/K_f-1)]-(2c_{11}^{(m)}+c_{33}^{(m)}+2c_{12}^{(m)}+4c_{13}^{(m)})/9}$, $m_i = \frac{\rho_f T_i}{\phi}$, $\Delta_i = \rho m_i - \rho_f^2$, $\Omega_i = \frac{\eta\phi^2\Lambda_i^2}{4T_i^2k_i^2\rho_f}$, $i = x,z$。$(D+\Omega_i)^{1/2}$, $i = x,z$ 是时域中的shifted fractional derivative operators with order 1/2.

Low ferquency

- 设计稳定、收敛、守恒的数值方法
- 方程(7)中，由于质点的速度大小和应力相差6个数量级,其本身是一个多尺度的问题
- 在低频的时候，如果孔隙间的流体是无粘的，则(7) 中的粘性项为**0**; 当有粘性的时候，粘性项(9) 有独立的特征衰减时间$\frac{\Delta_{x,z} k_{x,z}}{\rho\eta}$((9) 关于**Q** 求导得到的矩阵的特征值绝对值的倒数),不依赖计算时网格的大小，当计算时间步长远大于特征衰减时间时，就会是一个刚性问题. 在计算中，de la Puente (Geophys., 2008) 的文章以及Ou (SISC, 2013,2014)等文章中都是用算子分裂算法，先独立的求解粘性项再结合齐次的（7）进行计算的
- 我们用DG求解时，由于方法稳定性的要求，时间步长本身就很小(不发生时间步长远大于特征衰减时间），所以是直接算的（代价是计算时间长）。

High ferquency

在高频的时候，离散粘性项(10)中的分数阶导数是比较困难的，Lu (JCP, 2005) 和Chiavassa (JCP, 2011,2014, J. Acous. Soc. Amer. 2013) 引进记忆变量把分数阶导数化为整数阶导数进行计算的：

$$(D+\Omega_i)^{1/2}q_i(x,z,t) = \int_0^c \phi(y,t)dy + \int_c^\infty [\phi(y,t) - \kappa y^{2\alpha-3}(\Omega_i q_i(t) + \frac{\partial q_i(t)}{\partial t}]dy$$
$$+ \kappa \int_c^\infty y^{2\alpha-3}(\Omega_i q_i(t) + \dot{q}_i(t)]dy, \tag{11}$$

$$\phi(y,t) = \kappa \int_0^t e^{-(t-\tau)y^2-(t-\tau)\Omega}[\Omega_i q_x(\tau) + \frac{\partial q_i(t)}{\partial \tau}]d\tau, \tag{12}$$

$$\frac{\partial \phi(y,t)}{\partial t} = -(y^2+\Omega_i)\phi(y,t) + \kappa y^{2\alpha-1}[\Omega_i q_x(t) + \frac{\partial q_i(t)}{\partial t}], i = x, z. \tag{13}$$

然后第一项用Gauss-Jacobi数值积分计算，第二和第三项用shifted Laguerre计算：

$$(D+\lambda)^{1/2}q_i(t) = \sum_{i=1}^{Ng} w_i^{(Ng)}\phi(y_i^{(Ng)},t) + \sum_{i=1}^{Nl} w_i^{(Nl)}\phi(y_i^{(Nl)},t) + \Psi_l[\lambda q_i(t) + \frac{\partial q_i(t)}{\partial t}] \tag{14}$$

其中$\Psi_l = \kappa[1-\sum_{i=1}^{Nl} w_i^{(Nl)}(y_i^{Nl})^{-2}]$，$\kappa = 2sin(\pi/2)/\pi$。

High frequency

$$(D+\Omega_i)^{1/2}q_i(x,z,t)=\frac{1}{\pi}\int_0^\infty \frac{1}{\sqrt{\theta}}\psi_i(x,z,\theta,t)d\theta \tag{15}$$

$$\psi_i(x,z,\theta,t)=\int_0^t e^{-(\theta+\Omega_i)(t-\tau)}(\frac{\partial q_i}{\partial t}(x,z,\tau)+\Omega_i q_i(x,z,\tau))d\tau \tag{16}$$

$$\frac{\partial \psi_i}{\partial t}=-(\theta+\Omega_i)\psi_i+\frac{\partial q_i}{\partial t}+\Omega_i q_i \tag{17}$$

用数值积分得到：

$$(D+\Omega_i)^{\frac{1}{2}}q_i(x,z,t)\simeq\sum_{l=1}^N a_l^i\psi_l^i(x,z,\theta_l^i,t)\equiv\sum_{l=1}^N a_l^i\psi_l^i(x,z,t) \tag{18}$$

用优化的方法找到数值积分的权重和积分极点a_l和θ_l,从而处理了分数阶导数。

Mathematical models–high frequency

In high frequency, the dynamic permeability and tortuosity in frequency domain are approximated utilizing the multipoint Padé approximation for Stieltjes function. We use inverse Laplace transform to tortuosity and obtain the time domain governing equation without fractional derivatives where the convolution kernel is replaced by a finite number of memory variables satisfying local time ordinary differential equations. Thus the procedure for handling the system is much easier due to the absence of the fractional derivative.

Mathematical models–high frequency

We approximate the tortuosity as $\widetilde{\alpha}(\omega) \approx \frac{a}{-i\omega} + \alpha_\infty + \sum_{j=1}^{M'} \frac{r_j}{-i\omega - p_j}$ to obtain a new system

$$\partial_t \mathbf{Q} + \nabla \cdot \mathbf{F}(\mathbf{Q}) = \mathbf{h}(\mathbf{Q}) + \partial_t \mathbf{S} \tag{19}$$

where $\mathbf{Q} = (\tau_{xx}\ \tau_{zz}\ \tau_{xz}\ v_x\ v_z\ p\ q_x\ q_x\ \Theta^x_{1,\dots,M^x}\ \Theta^z_{1,\dots,M^z})^\top$ is the unknown vector, $\mathbf{F} = (\mathbf{f}, \mathbf{g})$ is the flux function, $\mathbf{h}(\mathbf{Q})$ is the viscous term, $\mathbf{S}$ again is external source.

$$\begin{aligned}
\mathbf{f}(\mathbf{Q}) = &-(c^u_{11} v_x + \alpha_1 M q_x, c^u_{13} v_x + \alpha_3 M q_x, c^u_{55} v_z, \frac{m_1}{\Delta_1}\tau_{xx} + \frac{\rho_f}{\Delta_1} p, \frac{m_3}{\Delta_3}\tau_{xz}, -\alpha_1 M v_x - M q_x, \\
&- \frac{\rho_f}{\Delta_1}\tau_{xx} - \frac{\rho}{\Delta_1} p, -\frac{\rho_f}{\Delta_3}\tau_{xz}, 0_1, \dots, 0_{M^x}, 0_1, \dots, 0_{M^z})^\top \\
\mathbf{g}(\mathbf{Q}) = &-(c^u_{13} v_z + \alpha_1 M q_z, c^u_{33} v_z + \alpha_3 M q_z, c^u_{55} v_x, \frac{m_1}{\Delta_1}\tau_{xz}, \frac{m_3}{\Delta_3}\tau_{zz} + \frac{\rho_f}{\Delta_3} p, -\alpha_3 M v_z - M q_z, \\
&- \frac{\rho_f}{\Delta_1}\tau_{xz}, -\frac{\rho_f}{\Delta_3}\tau_{zz} - \frac{\rho}{\Delta_3} p, 0_1, \dots, 0_{M^x}, 0_1, \dots, 0_{M^z})^\top
\end{aligned}$$

Mathematical models–high frequency

$$\mathbf{h}(\mathbf{Q}) = (0,0,0,(\frac{\rho_f\eta}{\Delta_1 k_1} + \frac{\rho_f^2}{\Delta_1\phi}\sum_{j=1}^{M_x} r_j^x)q_x - \frac{\rho_f^2}{\Delta_1\phi}\sum_{j=1}^{M^x} r_j^x\Theta_j^x, (\frac{\rho_f\eta}{\Delta_3 k_3} + \frac{\rho_f^2}{\Delta_3\phi}\sum_{j=1}^{M^z} r_j^z)q_z$$
$$-\frac{\rho_f^2}{\Delta_3\phi}\sum_{j=1}^{M^z} r_j^z\Theta_j^z, 0, -(\frac{\rho\eta}{\Delta_1 k_1} + \frac{\rho\rho_f}{\Delta_1\phi}\sum_{j=1}^{M^x} r_j^x)q_x + \frac{\rho\rho_f}{\Delta_1\phi}\sum_{j=1}^{M^x} r_j^x\Theta_j^x, -(\frac{\rho\eta}{\Delta_3 k_3}$$
$$+\frac{\rho\rho_f}{\Delta_3\phi}\sum_{j=1}^{M^z} r_j^z)q_z + \frac{\rho\rho_f}{\Delta_3\phi}\sum_{j=1}^{M^z} r_j^z\Theta_j^z, -p_1^x(q_x - \Theta_1^x), \ldots, -p_{M^x}^x(q_x - \Theta_{M_x}^x),$$
$$-p_1^z(q_z - \Theta_1^z), \ldots, -p_{M^z}^z(q_z - \Theta_{M_z}^z)\,)^\top$$

其中的记忆变量

$$\Theta_j(t) :\equiv (-p_j)\int_{-\infty}^{t} e^{p_j(t-\tau)}\mathbf{q}(\tau)d\tau, j = 1, \ldots M \qquad (20)$$

$$\partial_t\Theta_j^{x,z} = (-p_j^{x,z})[-\Theta_j^{x,z} + q^{x,z}(t)], j = 1, M^{x,z}. \qquad (21)$$

Example : **Point source in homogeneous medium**. We consider the problem that a homogeneous medium is excited by a source at the center.The computational domain is $\Omega_0 = [-0.15, 0.15]^2 m$, the source $S_3 = g(t)h(x, z)$ is only applied on τ_{xz}.

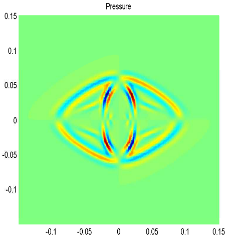

(a)

Figure: High frequency results in homogeneous medium, t=0.0000272s.(a)result from our model

Mathematical description

- Kinetic description (collisionless magnetized plasmas)
- Fluid description (collision magnetized plasmas)

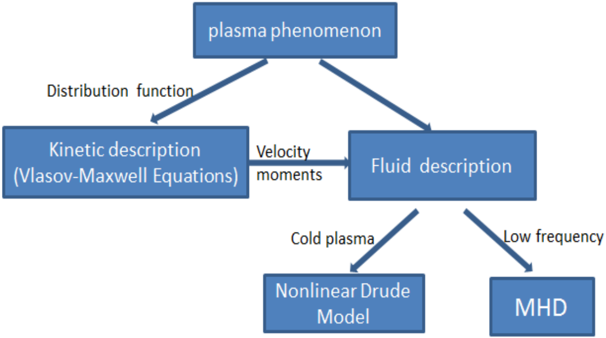

Ideal MHD equations

The ideal MHD equations consist of a system of nonlinear hyperbolic equations

$$\begin{aligned}
\frac{\partial \rho}{\partial t} + \nabla \cdot (\rho \mathbf{u}) &= 0\,, \\
\frac{\partial (\rho \mathbf{u})}{\partial t} + \nabla \cdot [\rho \mathbf{u}\mathbf{u}^\top + (p + \frac{1}{2}|\mathbf{B}|^2)\mathbf{I} - \mathbf{B}\mathbf{B}^\top] &= 0\,, \\
\frac{\partial \mathcal{E}}{\partial t} + \nabla \cdot [(\mathcal{E} + p + \frac{1}{2}|\mathbf{B}|^2)\mathbf{u} - \mathbf{B}(\mathbf{u}\cdot\mathbf{B})] &= 0\,, \\
\frac{\partial \mathbf{B}}{\partial t} + \nabla \times \mathbf{E} &= 0\,,
\end{aligned}$$

with an additional divergence-free constraint on the magnetic field

$$\nabla \cdot \mathbf{B} = 0\,.$$

ρ: density, $\mathbf{u} = (u_x, u_y, u_z)^\top$: velocity field, $\mathbf{B} = (B_x, B_y, B_z)^\top$: magnetic field. $\mathcal{E}$: total energy, $\mathbf{E} = -\mathbf{u} \times \mathbf{B}$: electric field, $\mathbf{I}$: identity matrix, $\nabla\cdot$ is the divergence operator, $\nabla\times$ is the curl operator, γ: ratio of specific heats, and p: pressure given by

$$p = (\gamma - 1)(\mathcal{E} - \frac{1}{2}\rho|\mathbf{u}|^2 - \frac{1}{2}|\mathbf{B}|^2)\,.$$

Zhang's PP limiter for Euler equations (Zhang et al. 2010)

Consider 1D Euler system:

$$\frac{\partial \mathbf{U}}{\partial t} + \frac{\partial \mathbf{f}(\mathbf{U})}{\partial x} = \mathbf{0} \tag{22}$$

where $\mathbf{U} = (\rho, \rho u, E)^T, \mathbf{f}(\mathbf{U}) = (\rho u, \rho u^2 + p, u(E+p), p(\mathbf{U}) = (\gamma - 1)(E - \frac{1}{2}\rho u^2)$;

Define an admissible set $G = \{\mathbf{U} : \rho > 0 \text{ and } p(\mathbf{U}) > 0\}$,

assume $\mathbf{U}_j^n, \mathbf{U}_{j-1}^n, \mathbf{U}_{j+1}^n \in G$, by introducing the Lax-Friedriches numerical flux

$$\mathbf{h}(\mathbf{U}, \mathbf{V}) = \frac{1}{2}[\mathbf{f}(\mathbf{U}) + \mathbf{f}(\mathbf{V}) - a_0^E(\mathbf{V} - \mathbf{U})], a_0^E = \| \ (|u_x| + c) \ \|_\infty,$$

the first order finite volume scheme can be written as

$$\begin{aligned} \mathbf{U}_j^{n+1} &= \mathbf{U}_j^n - \lambda[\mathbf{h}(\mathbf{U}_j^n, \mathbf{U}_{j+1}^n) - \mathbf{h}(\mathbf{U}_{j-1}^n, \mathbf{U}_j^n)] \\ &= (1 - \lambda a_0^E)\mathbf{U}_j^n + \frac{\lambda a_0^E}{2}[\mathbf{U}_{j+1}^n - \frac{1}{a_0^E}\mathbf{f}(\mathbf{U}_{j+1}^n)] + \frac{\lambda a_0^E}{2}[\mathbf{U}_{j-1}^n + \frac{1}{a_0^E}\mathbf{f}(\mathbf{U}_{j-1}^n)] \end{aligned} \tag{23}$$

then that the flux splitting terms $\mathbf{U}_{j+1}^n - \frac{1}{a_0^E}\mathbf{f}(\mathbf{U}_{j+1}^n), \mathbf{U}_{j-1}^n + \frac{1}{a_0^E}\mathbf{f}(\mathbf{U}_{j-1}^n) \in G$ can be rigorously proved and hence, a **1D first order PP** Lax-Friedriches scheme can be obtained under $\lambda a_0^E \leq 1$. Design of high-order 1D PP scheme and generalization to multi-dimensional case can be successfully processed

Zhang's PP limiter for ideal MHD equations (X. et al. 2013)

With $\mathbf{U} = (\rho, \rho u, B_x, E)^T$, the 1D ideal MHD equations reads

$$\frac{\partial \mathbf{U}}{\partial t} + \frac{\partial \mathbf{f}(\mathbf{U})}{\partial x} = \mathbf{0}$$

$$\mathbf{f}(\mathbf{U}) = (\rho u, \rho u^2 + p - \tfrac{1}{2}B_x^2, 0, u(E + p - \tfrac{1}{2}B_x^2)), \quad p(\mathbf{U}) = (\gamma - 1)(E - \tfrac{1}{2}\rho u^2 - \tfrac{1}{2}B_x^2)$$

$$p\left(\mathbf{U} \pm \frac{\mathbf{f}(\mathbf{U})}{a_0^M}\right) > 0 \iff \frac{(p - \frac{1}{2}B_x^2)^2}{\rho(a_0^M \pm u)^2} < \frac{2p}{\gamma - 1} \pm \frac{u}{a_0^M \pm u} B_x^2 \tag{24}$$

However,the inequality (24) does not necessarily hold. For example,$\forall p > 0$,take an admissible state $\mathbf{U} = (\rho, \rho u, B_x, E) = (1, 0, 1, \frac{p}{\gamma - 1} + \frac{1}{2}) \in G$,then (24) reduces to $\frac{(p - \frac{1}{2})^2}{(a_0^M)^2} < \frac{2p}{\gamma - 1}$ which may not be true when $p \to 0+$.

A new simple and conservative PP limiter for ideal MHD equations

Reformulating the 1D first order Lax-Friedriches scheme (23) as

$$\begin{aligned} \mathbf{U}_j^{n+1} &= \mathbf{U}_j^n - \lambda[\mathbf{h}(\mathbf{U}_j^n, \mathbf{U}_{j+1}^n) - \mathbf{h}(\mathbf{U}_{j-1}^n, \mathbf{U}_j^n)] \\ &= (1 - \lambda a)\mathbf{U}_j^n + \frac{\lambda}{2}\left[a\mathbf{U}_{j+1}^n - \mathbf{f}(\mathbf{U}_{j+1}^n) + a\mathbf{U}_{j-1}^n + \mathbf{f}(\mathbf{U}_{j-1}^n)\right] \end{aligned} \tag{25}$$

By introducing the *Hadamard product* $\circ$ and taking the viscosity parameter $\mathbf{a} \in \mathbb{R}^4$ as a vector, scheme (25) takes the following form

$$\mathbf{U}_j^{n+1} = (1 - \lambda\mathbf{a}\circ)\mathbf{U}_j^n + \frac{\lambda}{2}\left[\mathbf{a} \circ \mathbf{U}_{j+1}^n - \mathbf{f}(\mathbf{U}_{j+1}^n) + \mathbf{a} \circ \mathbf{U}_{j-1}^n + \mathbf{f}(\mathbf{U}_{j-1}^n)\right], \tag{26}$$

$$\forall \mathbf{U} \in G, \mathbf{U} - \lambda\mathbf{a} \circ \mathbf{U} \in G \textit{ and } \forall \mathbf{U} \in G, \mathbf{a} \circ \mathbf{U} \pm \mathbf{f}(\mathbf{U}) \in G$$

A new simple and conservative PP limiter for ideal MHD equations

Lemma

Let $\mathbf{U} = (\rho, \rho u, B_x, E)^T$,$\mathbf{f}(\mathbf{U}) = (\rho u, \rho u^2 + p - \frac{1}{2}B_x^2, 0, u(E + p - \frac{1}{2}B_x^2)$,$\mathbf{a} = (\alpha, \alpha, \beta, \alpha)$, *then for any* $\mathbf{U} \in G$*, we have* $\mathbf{a} \circ \mathbf{U} \pm \mathbf{f}(\mathbf{U}) \in G$ *if*

$$\alpha > |u| + \frac{\rho\beta^2 B_x^2 + \sqrt{\rho^2\beta^4 B_x^4 + 2\rho(2E - \rho u^2)(2p - B_x^2)^2}}{2\rho(2E - \rho u^2)} \tag{27}$$

Proof.

For any vector $\mathbf{U} = (\rho, \rho u, B_x, E)^T$, define the function $\chi(\mathbf{U}) = \frac{\rho p}{\gamma - 1} = \rho E - \frac{1}{2}\rho u^2 - \frac{1}{2}\rho B_x^2$. We only need to show that $\chi\left[\mathbf{a} \circ \mathbf{U} \pm \mathbf{f}(\mathbf{U})\right] > 0$ since the first component of $\mathbf{a} \circ \mathbf{U} \pm \mathbf{f}(\mathbf{U})$ is positive once (27) holds. Denote $\bar{\alpha} = \alpha \pm u$, then after a direct calculation, we have a quadratic form of $\bar{\alpha}$:

$$\begin{aligned}
\chi\left[\mathbf{a} \circ \mathbf{U} \pm \mathbf{f}(\mathbf{U})\right] &= \chi\left[\rho\bar{\alpha}, \rho u\bar{\alpha} \pm (p - \frac{1}{2}B_x^2), \beta B_x, E\bar{\alpha} \pm (p - \frac{1}{2}B_x^2)u\right] \\
&= \rho(E - \frac{1}{2}\rho u^2)\bar{\alpha}^2 - \frac{1}{2}\rho\beta^2 B_x^2\bar{\alpha} - \frac{1}{2}(p - \frac{1}{2}B_x^2)^2
\end{aligned}$$

Since $\mathbf{U} \in G$, we have a positive quadratic term $\rho(E - \frac{1}{2}\rho u^2) > 0$ therefore $\chi\left[\mathbf{a} \circ \mathbf{U} \pm \mathbf{f}(\mathbf{U})\right] > 0$ if α satisfies (27).

A new simple and conservative PP limiter for ideal MHD equations

Lemma

And we have $\mathbf{U} - \lambda \mathbf{a} \circ \mathbf{U} \in G$ if $\lambda\beta$ is less than some positive number.

Proof.

We first have $\mathbf{U} - \lambda \mathbf{a} \circ \mathbf{U} = ((1-\lambda\alpha)\rho, (1-\lambda\alpha)\rho u, (1-\lambda\beta)B_x, (1-\lambda\alpha)E)^T$. Thus we need $\chi(\mathbf{U} - \lambda \mathbf{a} \circ \mathbf{U}) > 0$.After simplification, we have a quadratic form of $\xi = \lambda\beta$:

$$-\frac{1}{2}B_x^2\xi^2 + \left(B_x^2 - \frac{\alpha}{\beta}(E - \frac{1}{2}\rho u^2)\right)\xi + (E - \frac{1}{2}\rho u^2 - \frac{1}{2}B_x^2) > 0$$

The two roots are $\xi_i = \frac{B_x^2 - \frac{\alpha}{\beta}(E - \frac{1}{2}\rho u^2) \pm \sqrt{\left[B_x^2 - \frac{\alpha}{\beta}(E - \frac{1}{2}\rho u^2)\right]^2 + 2B_x^2(E - \frac{1}{2}\rho u^2 - \frac{1}{2}B_x^2)}}{B_x^2}$, $i = 1, 2$.
One of them must be positive as $\xi_1\xi_2 < 0$. □

Design of 1D high order PP scheme and generalization to multidimensional case follow Zhang's PP scheme.Note that our overall PP scheme is simple, unlike Wu's PP scheme, there is no need to consider the divergence free condition.

Blast problem

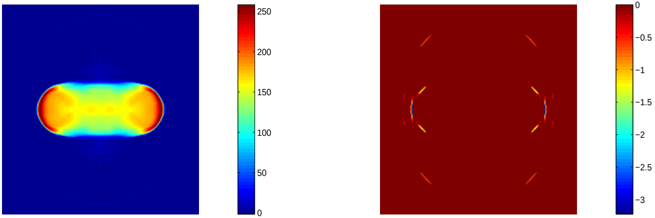

Figure: P^3 approximation of the pressure in the blast problem on the 200×200 mesh at $t = 0.01$. Left: pressure p; Right: $\min(0, p)$.

Blast problem

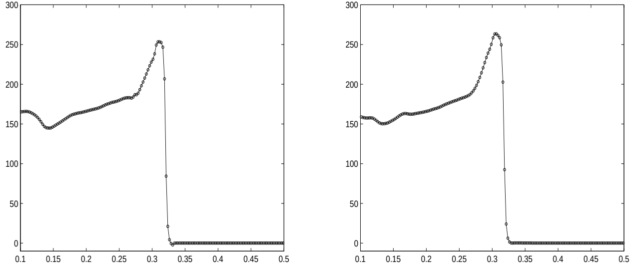

Figure: Solution slice of pressure p for the blast problem at $t = 0.01$ with $y = 0.0$ on a 400×400 mesh. Left: base DG method; right: positivity-preserving DG method.

We consider the incompressible MHD equations

$$\mu\partial_t\mathbf{H} + \sigma^{-1}\nabla\times(\nabla\times\mathbf{H}) - \mu\nabla\times(\mathbf{u}\times\mathbf{H}) = \sigma^{-1}\nabla\times J \tag{28}$$
$$\partial_t\mathbf{u} + (\mathbf{u}\cdot\nabla)\mathbf{u} - \nu\Delta\mathbf{u} + \nabla p = \mathbf{f} - \mu\mathbf{H}\times(\nabla\times\mathbf{H}) \tag{29}$$
$$\nabla\cdot\mathbf{u} = 0 \tag{30}$$

in a polygonal type domain $\Omega = \Omega_0 \backslash (\cup_{j=1}^m \Omega_j)$, where both Ω_0 and $\Omega_j \subset \Omega_0$, $j = 1, \ldots, m$, are polygons. In the system (28)-(30), $\mathbf{u}$ denotes the velocity field, $\mathbf{H}$ the magnetic field, p the pressure, $\mathbf{f}$ and J the given source terms; μ, ν and σ are physical constants. The boundary conditions

$$\mathbf{H}\cdot\mathbf{n} = 0, \quad \nabla\times\mathbf{H} = J, \quad \text{and} \quad \mathbf{u} = 0 \quad \text{on } \partial\Omega\times(0,T] \tag{31}$$

and the initial condition

$$\mathbf{H}|_{t=0} = \mathbf{H}_0 \quad \text{and} \quad \mathbf{u}|_{t=0} = u_0 \quad \text{in } \Omega. \tag{32}$$

Notations

The following 2D notations of curl, divergence and gradient operators are used for any vectors field $\mathbf{B} = (B_1, B_2)$ and scalar field ψ:

$$\nabla \times \mathbf{B} = \frac{\partial B_2}{\partial x_1} - \frac{\partial B_1}{\partial x_2} \qquad \nabla \cdot \mathbf{B} = \frac{\partial B_1}{\partial x_1} + \frac{\partial B_2}{\partial x_2}$$

$$\nabla \times \psi = \left(\frac{\partial \psi}{\partial x_2} \quad -\frac{\partial \psi}{\partial x_1}\right) \quad \nabla \psi = \left(\frac{\partial \psi}{\partial x_1}, \frac{\partial \psi}{\partial x_2}\right).$$

Issues for approximating incompressible MHD equations

The challenges to design accurate, robust and efficient numerical methods mainly consist of:

- The irregularity on geometry in real-word electromagnetic problems leads to low regularity of true solutions, and this yields special challenges on the design and analysis of numerical schemes. For instance, the Lipschitz polyhedron domain (possibly non-convex) in $\mathbb{R}^d$ ($d = 2, 3$) and perfectly conducting wall boundary condition can only guarantee H^s regularity for the magnetic field $\mathbf{H}$, with $s \in (\frac{1}{2}, 1]$.

- The incompressible conditions for velocity $\mathbf{u}$ and magnetic field $\mathbf{H}$ are important in physical, therefore, numerical schemes which can preserve this condition may be considered as a good scheme.

- Our work here: a linearized Lagrange FEM for the incompressible MHD equations without the assumption on the sufficient smoothness of weak solutions.

An equivalent form

Thus, instead of solving (28)-(29) directly, we propose to solve the following equations:

$$\mu\partial_t A - \sigma^{-1}\Delta A - \mu\mathbf{u} \times (\nabla \times A) = \sigma^{-1}J \tag{33}$$

$$\partial_t\mathbf{u} + (\mathbf{u}\cdot\nabla)\mathbf{u} - \nu\Delta\mathbf{u} + \nabla p = \mathbf{f} + \mu(\nabla \times A) \times \Delta A \tag{34}$$

$$\nabla \cdot \mathbf{u} = 0 \tag{35}$$

with the boundary conditions

$$\mathbf{u} = 0, \quad A = 0 \quad \text{on } \partial\Omega \times (0, T] \tag{36}$$

and the initial condition

$$\mathbf{u}|_{t=0} = u_0 \quad \text{and} \quad A|_{t=0} = A_0 \quad \text{in } \Omega, \tag{37}$$

where A_0 is the solution of

$$\begin{cases} -\Delta A_0 = \nabla \times \mathbf{H}_0 & \text{in } \Omega, \\ A_0 = 0 & \text{on } \partial\Omega. \end{cases} \tag{38}$$

After solving (33)-(35), we can obtain the magnetic field $\mathbf{H} = \nabla \times A$.

A FEM method

A fully discrete numerical scheme for the system (33)-(35) is to find $A_h^n \in S_h^{r+1}$, $\mathbf{u}_h^n \in S_h^{r+1} \times S_h^{r+1}$ and $p_h^n \in S_h^r$ such that

$$\left(\mu \frac{A_h^n - A_h^{n-1}}{\tau}, a_h\right) + (\sigma^{-1}\nabla A_h^n, \nabla a_h) - (\mu \mathbf{u}_h^n \times (\nabla \times A_h^{n-1}), a_h) = (\sigma^{-1} J^n, a_h), \tag{39}$$

$$\left(\frac{\mathbf{u}_h^n - \mathbf{u}_h^{n-1}}{\tau}, \mathbf{v}_h\right) + \frac{1}{2}(\mathbf{u}_h^{n-1} \cdot \nabla \mathbf{u}_h^n, \mathbf{v}_h) - \frac{1}{2}(\mathbf{u}_h^{n-1} \cdot \nabla \mathbf{v}_h, \mathbf{u}_h^n) + (\nu \nabla \mathbf{u}_h^n, \nabla \mathbf{v}_h) - (p_h^n, \nabla \cdot \mathbf{v}_h)$$
$$= (\mathbf{f}^n, \mathbf{v}_h) + (\mu(\nabla \times A_h^{n-1}) \times \Delta_h A_h^n, \mathbf{v}_h), \tag{40}$$
$$(\nabla \cdot \mathbf{u}_h^n, q_h) = 0, \tag{41}$$

hold for all test functions $a_h \in \mathring{S}_h^{r+1}$, $\mathbf{v}_h \in \mathring{\mathbf{S}}_h^{r+1}$ and $q_h \in S_h^r$. The operator $\Delta_h : \mathring{S}_h^{r+1} \to \mathring{S}_h^{r+1}$ is defined via the duality:

$$(\Delta_h A_h^n, a_h) = -(\nabla A_h^n, \nabla a_h) \quad \forall a_h \in \mathring{S}_h^{r+1}. \tag{42}$$

For any sequence ω_h^n, $n = 1, 2, \ldots,$ we define the piecewise constant functions $\omega_{h,\tau}^+$ and $\omega_{h,\tau}^-$ by

$$\omega_{h,\tau}^+(t) := \omega_h^n \quad \text{and} \quad \omega_{h,\tau}^-(t) := \omega_h^{n-1} \tag{43}$$

for $t \in [t_{n-1}, t_n]$ and $n = 1, 2, \ldots, N$.

Main convergence results

Theorem

Assume that the PDE problem (33)-(38) *has a unique weak solution. Then the fully discrete finite element method* (39)-(41) *has a unique solution, which converges to the weak solution of the PDE problem as* $h \to 0$ *and* $\tau \to 0$ *in the following sense:*

$$A^{+}_{h,\tau} \ \textit{converges to } A \textit{ strongly in } \ L^2(0,T;H^1(\Omega)), \tag{44}$$

$$\mathbf{u}^{+}_{h,\tau} \ \textit{converges to } \mathbf{u} \textit{ strongly in } \ L^2(0,T;L^2(\Omega)). \tag{45}$$

非线性动力学Drude模型

对金属纳米结构做自由电子气体近似，从流体动力学角度有：

- 电荷守恒：

$$\frac{\partial(n_e q_e)}{\partial t} + \nabla \cdot (n_e q_e \mathbf{u}_e) = 0, \mathbf{x} \in \Omega_2,$$

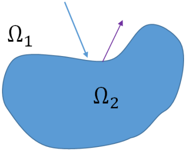

- 动量平衡(牛顿第二定律)：

$$m_e \left[\frac{\partial \mathbf{u}_e}{\partial t} + (\mathbf{u}_e \cdot \nabla)\mathbf{u}_e\right] = q_e(\mathbf{E} + \mu_0 \mathbf{u}_e \times \mathbf{H}) - \frac{1}{\tau} m_e \mathbf{u}_e - \nabla \frac{\delta g[n_e]}{\delta n_e}, \mathbf{x} \in \Omega_2,$$

其中$\delta g[n_e]$表示内部能量泛函（包括动能，交换-关联势能）

Thomas-Fermi 动能近似（忽略交换-关联势能）

$$\frac{\delta g[n_e]}{\delta n_e} \approx p = (3\pi^2)^{2/3}(\hbar^2/5m_e)n_e^{5/3}$$

非线性动力学Drude模型

定义
电荷密度：$\rho = n_e q_e$
电流密度：$\mathbf{J} = \rho \mathbf{u_e}$

非线性动力学Drude模型:

$$
\begin{aligned}
\mu_0 \frac{\partial \mathbf{H}}{\partial t} + \nabla \times \mathbf{E} &= \mathbf{0}, \\
\epsilon_0 \frac{\partial \mathbf{E}}{\partial t} - \nabla \times \mathbf{H} &= -\mathbf{J}, \mathbf{x} \in \Omega_1 \cup \Omega_2. \\
\frac{\partial \rho}{\partial t} + \nabla \cdot \mathbf{J} &= 0, \\
\frac{\partial \mathbf{J}}{\partial t} + \nabla \cdot (\rho \mathbf{u_e} \otimes \mathbf{u_e}) &= \frac{q_e}{m_e}(\rho \mathbf{E} + \mu_0 \mathbf{J} \times \mathbf{H}) - \frac{1}{\tau}\mathbf{J} - \frac{q_e}{m_e}\nabla p, \mathbf{x} \in \Omega_2
\end{aligned}
$$

非局域动力学Drude模型

对电荷密度$n_e(\mathbf{x},t)$进行线性化：$n_e(\mathbf{x},t)=n_0+n_1(\mathbf{x},t)$,则

$$\begin{aligned}\nabla\left(\frac{\delta g[n_e]}{\delta n_e}\right) &\approx m_e\beta^2\frac{\nabla n_1}{n_0},\beta^2=\frac{3}{5}v_F^2\\ \frac{\partial n_1}{\partial t}+n_0\nabla\cdot\mathbf{u}_e &= 0\end{aligned}$$

去掉动量平衡方程中的非线性项$(\mathbf{u}_e\cdot\nabla)\mathbf{u}_e$和$\mathbf{u}_e\times\mathbf{H}$ 后得到

$$\frac{\partial^2\mathbf{J}}{\partial t^2}+\beta^2\nabla(\nabla\cdot\mathbf{J})=\omega_p^2\epsilon_0\frac{\partial\mathbf{E}}{\partial t}-\frac{1}{\tau}\frac{\partial\mathbf{J}}{\partial t},\mathbf{x}\in\Omega_2$$

非局域动力学Drude模型

$$\begin{aligned}\frac{\partial\mathbf{H}}{\partial t}+\nabla\times\mathbf{E} &= \mathbf{0},\\ \frac{\partial\mathbf{E}}{\partial t}-\nabla\times\mathbf{H} &= -\mathbf{J},\mathbf{x}\in\Omega_1\cup\Omega_2;\\ \frac{\partial\mathbf{J}}{\partial t}-\beta^2\nabla Q &= \omega_p^2\mathbf{E}-\frac{1}{\tau}\mathbf{J},\\ \frac{\partial Q}{\partial t}-\nabla\cdot\mathbf{J} &= 0,\mathbf{x}\in\Omega_2.\end{aligned}$$

局域动力学Drude模型

$$\begin{aligned}\frac{\partial\mathbf{H}}{\partial t}+\nabla\times\mathbf{E} &= \mathbf{0},\\ \frac{\partial\mathbf{E}}{\partial t}-\nabla\times\mathbf{H} &= -\mathbf{J},\mathbf{x}\in\Omega_1\cup\Omega_2;\\ \frac{\partial\mathbf{J}}{\partial t} &= \omega_p^2\mathbf{E}-\frac{1}{\tau}\mathbf{J},\mathbf{x}\in\Omega_2.\end{aligned}$$

其中$\omega_p=\sqrt{\frac{n_0q_e^2}{m_e\epsilon_0}}$为等离子体本征频率。

频域线性Drude模型

$$
\begin{aligned}
\nabla \times \nabla \times \mathbf{E} - \omega^2 \mathbf{E} &= i\omega \mathbf{J},\ \mathbf{x} \in \Omega_1 \cup \Omega_2 \\
\beta^2 \nabla(\nabla \cdot \mathbf{J}) + \omega(\omega + i\gamma)\mathbf{J} &= i\omega {\omega_p}^2 \mathbf{E},\ \mathbf{x} \in \Omega_2, \\
\mathbf{n} \cdot \mathbf{J} &= 0,\ \mathbf{x} \in \partial\Omega_2 \\
\nu \times \nabla \times \mathbf{E} &= \mathcal{T}\mathbf{E}, \mathbf{x} \in \Gamma
\end{aligned}
$$

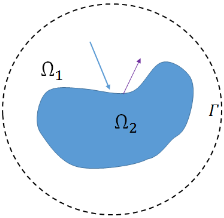

- 使用旋度和散度协调有限元求解(K. R. Hiremath *et al*, 2012, JCP)

线性Drude模型($\beta = 0$):

$$
\begin{aligned}
\nabla \times \mathbf{H} &= -i\omega\epsilon_0 \mathbf{E} + \mathbf{J},\ \mathbf{x} \in \Omega_1 \cup \Omega_2 \\
\nabla \times \mathbf{E} &= -i\omega\epsilon_0 \mathbf{H},\ \mathbf{x} \in \Omega_1 \cup \Omega_2 \\
\beta^2 \nabla(\nabla \cdot \mathbf{J}) + \omega(\omega + i\gamma)\mathbf{J} &= i\omega {\omega_p}^2 \mathbf{E},\ \mathbf{x} \in \Omega_2
\end{aligned}
$$

$$
\nabla \times \nabla \times \mathbf{E} - k^2 \mathbf{E} = 0,
$$

$$
k^2 = \omega^2 + \frac{\omega\omega_p^2}{\omega + i\gamma}
$$

- 利用HDG求解并证明了解的唯一性(F. Vidal-Codina *et al*, 2018, JCP)

数值模拟挑战性

- 强非线性：电子流体速度对流，所受洛伦兹力和量子压力使得整个模型具有强非线性
- 多物理场耦合（边界条件处理）：运动流体+电磁场
- 间断：电子密度ρ在金属表面的强间断（电场的法向和磁场切向不连续）
- 多尺度：电磁场激发强度和产生的非线性响应强度相差大(10^7)
- 区域无界性：完美匹配层吸收
- 数值稳定性：高精度长时间模拟

数值算例

精度测试： 考虑TM模式下的非线性动力学Drude模型

$$\begin{pmatrix} H_z \\ E_x \\ E_y \end{pmatrix}_t + \begin{pmatrix} E_y \\ 0 \\ H_z \end{pmatrix}_x + \begin{pmatrix} -E_x \\ -H_z \\ 0 \end{pmatrix}_y = \begin{pmatrix} 0 \\ -\rho u_x \\ -\rho u_y \end{pmatrix} - \tilde{\mathbf{S}}_1^a$$

$$\begin{pmatrix} \rho \\ \rho u_x \\ \rho u_y \end{pmatrix}_t + \begin{pmatrix} \rho u_x \\ \rho u_x^2 \\ \rho u_x u_y \end{pmatrix}_x + \begin{pmatrix} \rho u_y \\ \rho u_x u_y \\ \rho u_y^2 \end{pmatrix}_y = \rho \begin{pmatrix} 0 \\ \frac{q_e}{m_e}(E_x + u_y H_z) - \frac{1}{\tau} u_x \\ \frac{q_e}{m_e}(E_y - u_x H_z) - \frac{1}{\tau} u_y \end{pmatrix} - \tilde{\mathbf{S}}_2^a$$

x,y方向采用周期边界条件，在$[0,1] \times [0,1]$上有精确解$(\rho, u_x, u_y) = [1 + 0.5sin2\pi(x + y - 2t), 1, 1], (H_z, E_x, E_y) = e^{cos2\pi(t/\alpha + x + y)}[1, \alpha, -\alpha]$
$\alpha = \frac{\sqrt{2}}{2}, \frac{q_e}{m_e} = 1, \tau = 1$。

Mesh	ρ		H_z		E_x		E_y	
	L^2 error	Order	L^2 error	Order	L^2 error	Order	L^2 error	Order
P^1								
10	0.99E-01	-	0.17E+00	-	0.13E+00	-	0.13E+00	-
20	0.15E-01	2.71	0.47E-01	1.86	0.34E-01	1.87	0.35E-01	1.92
40	0.22E-02	2.81	0.82E-02	2.50	0.62E-02	2.46	0.62E-02	2.47
80	0.36E-03	2.61	0.13E-02	2.67	0.11E-02	2.56	0.11E-02	2.56
160	0.72E-04	2.30	0.23E-03	2.47	0.21E-03	2.31	0.21E-03	2.31
P^2								
10	0.58E-02	-	0.27E-01	-	0.20E-01	-	0.20E-01	-
20	0.58E-03	3.32	0.21E-02	3.65	0.17E-02	3.51	0.17E-02	3.51
40	0.53E-04	3.45	0.18E-03	3.57	0.17E-03	3.34	0.17E-03	3.37
80	0.55E-05	3.27	0.20E-04	3.16	0.20E-04	3.06	0.20E-04	3.08
160	0.77E-06	2.84	0.24E-05	3.03	0.25E-05	3.00	0.25E-05	3.01

数值算例

线性响应： 考虑参数为$v_F = 1.07 \times 10^6 m/s, \omega_p = 8.65 \times 10^{15} s^{-1}, \gamma = 1/\tau = 0.01\omega_p$的无限长银圆柱。xy方向采用PML 截断，总场/散射场分离技术引入正弦函数调制的高斯平面脉冲。分别计算（a）半径200nm银圆柱的局域线性响应，表明此时电磁波主要向前散射，与解析Mie级数解吻合；（b）半径2nm银圆柱线性局域和非局域响应，观察到金属表面响应蓝移和多频内部响应非局域现象，与解析Mie 级数解吻合；（c）半径2∼10nm银圆柱非局域现象，结果表明，非局域响应强度（表面响应蓝移和内部多频共振）随着纳米结构尺寸增大而减弱，接近10nm时与局域响应几乎相同。

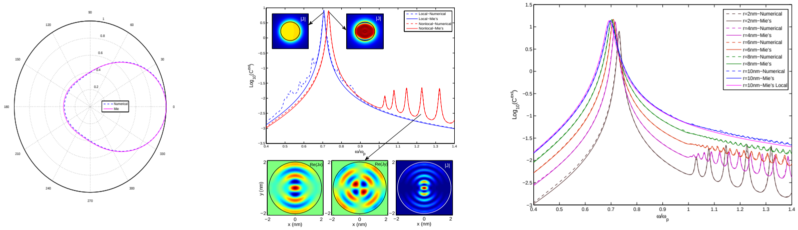

(a) (b) (c)

Figure: (a)200nm银圆柱雷达散射截面(b) 2nm银圆柱消光散射截面(c) 2∼10nm银圆柱消光散射截面.

数值算例

非线性响应： 考虑2.5维下参数为$\omega_p = 1.367 \times 10^{16} s^{-1}, \tau = 15.44 fs$的x方向上周期排列的金属纳米结构阵列，采用硬源技术y 方向引入载入波长为$\lambda = 1200\ nm$的正弦调制高斯平面脉冲。x 方向采用周期边界条件，y方向采用PML进行截断，分别模拟非对称L型纳米结构和对称矩形纳米结构的高次谐波产生现象。

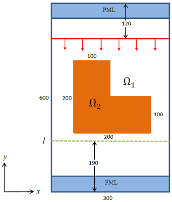

(a)

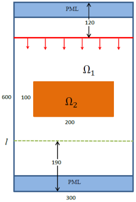

(b)

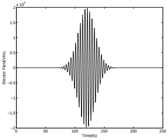

(c)

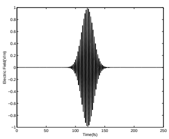

(d)

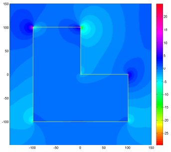

(e)

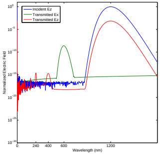

(f)

Figure: (c) 线性响应(d) L型结构二次谐波; (e) 二次谐波电场, (f) L型结构响应频谱，可以发现不仅能产生二次谐波，三次、五次谐波也可以模拟出来。

对称矩形结构：

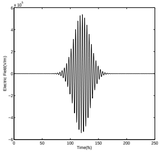

(a)

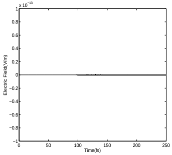

(b)

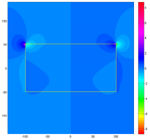

(c)

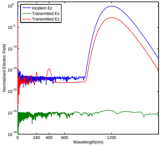

(d)

Figure: (a) 线性响应(b) 矩形结构二次谐波; (c) 二次谐波电场; (d) 矩形结构响应频谱。二次谐波电场严格对称性使得二次谐波不能产生，但是三次，五次谐波仍然可以产生。

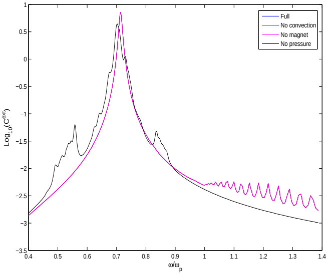

Figure: 利用非线性动力学Drude模型计算2nm无限长银圆柱的消光散射截面。不同颜色线表示去掉对流项，磁力项，压力项对非局域响应产生的影响（蓝色包含所有因素），结果表明只有压力项才能对非局域效应（内部多频共振和表面响应蓝移）产生影响。

Central discontinuous Galerkin (CDG) methods

- Review of CDG method
- Development of CDG method
  - Physical-constraint-preserving schemes
    - Divergence-free CDG method
    - Maximum-principle-satisfying CDG method
    - Positivity-preserving CDG method
    - Well-balanced CDG method
  - Fast and feasible schemes
    - Reconstructed CDG method
    - CDG method on unstructured overlapping meshes
- Numerical results

Introduction of CDG method

Overlapping meshes: let $\{x_j\}_j$ be a partition of the domain Ω, and $x_{j-1/2} = \frac{1}{2}(x_{j-1} + x_j)$

Primal mesh (C): $\{I_j = (x_{j-\frac{1}{2}}, x_{j+\frac{1}{2}})\}_j$; Dual mesh (D): $\{I_{j+1/2} = (x_j, x_{j+1})\}_j$

Discrete function spaces: $\mathcal{V}_h^C = \mathcal{V}_h^{C,k} = \{\nu : \nu|_{I_j} \in (P^k(I_j))^2, \forall\, j\}$

$$\mathcal{V}_h^D = \mathcal{V}_h^{D,k} = \{\nu : \nu|_{I_{i+\frac{1}{2}}} \in (P^k(I_{j+\frac{1}{2}}))^2, \forall\, j\}$$

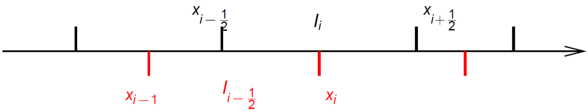

Introduction of CDG method

Consider the conservation law

$$u_t + F(u)_x = 0 \,, \tag{46}$$

The standard CDG method (*Liu-Shu-Tadmor-Zhang (2007,2008,2011)*) for (46) is given by: Look for $u_h^{n+1,\star} \in \mathcal{V}_h^\star$, such that $\forall v^\star \in \mathcal{V}_h^\star$ with any j and $\star = C, D$,

$$\begin{aligned} \int_{I_j} u_h^{n+1,C} v^C dx &= \int_{I_j} \left(\theta_n u_h^{n,D} + (1-\theta_n) u_h^{n,C}\right) v^C dx + \Delta t_n \int_{I_j} F(u_h^{n,D}) v_x^C dx \\ &- \Delta t_n \left[F(u_h^{n,D}(x_{j+\frac{1}{2}})) v^C(x_{j+\frac{1}{2}}^-) - F(u_h^{n,D}(x_{j-\frac{1}{2}})) v^C(x_{j-\frac{1}{2}}^+) \right] \,, \end{aligned} \tag{47}$$

$$\begin{aligned} \int_{I_{j-\frac{1}{2}}} u_h^{n+1,D} v^D dx &= \int_{I_{j-\frac{1}{2}}} \left(\theta_n u_h^{n,C} + (1-\theta_n) u_h^{n,D}\right) v^D dx + \Delta t_n \int_{I_{j-\frac{1}{2}}} F(u_h^{n,C}) v_x^D dx \\ &- \Delta t_n \left[F(u_h^{n,C}(x_j)) v^D(x_j^-) - F(u_h^{n,D}(x_{j-1})) v^D(x_{j-1}^+) \right] \,. \end{aligned} \tag{48}$$

Here $\theta_n = \Delta t_n / \tau \in (0,1]$, with τ being the maximal time step allowed by the CFL restriction.

Development of CDG methods

- CDG method on overlapping meshes for conservation laws [Y Liu, et al., 2007,2008]
- CLDG method for diffusion equations [Y Liu, et al., 2011]
- Divergence-free CDG method on unstructured meshes for MHD equations [Y Liu, et al., 2016]
- Divergence-free CDG method for MHD equations [F Li, et al., 2011, 2012,2013]
- Positivity-preserving CDG method for MHD equations [X., et al., 2013]
- Physical-constraint-preserving CDG method for conservation laws [X., et al., 2016]
- Well-balanced and Positivity-preserving CDG method for shallow water (Green-Naghdi) equations [X., et al., 2014,2017]
- Reconstructed CDG methods [Li, et al., 2016, 2017]
- CDG methods on unstructured grids [X., et al., 2018]

Reconstructed CDG method

The reconstructed CDG method is as follows: looking for $u_h^{n+1,\star} \in \mathcal{V}_h^\star$, such that for any $v^\star \in \mathcal{V}_h^\star$ with any j,

$$\begin{aligned}\int_{I_j} u_h^{n+1,C} v^C dx &= \int_{I_j} \left(\theta_n u_h^{n,D} + (1-\theta_n) u_h^{n,C}\right) v^C dx + \Delta t_n \int_{I_j} F(u_h^{n,D}) v_x^C dx \\ &- \Delta t_n \left[F(u_h^{n,D}(x_{j+\frac{1}{2}})) v^C(x_{j+\frac{1}{2}}^-) - F(u_h^{n,D}(x_{j-\frac{1}{2}})) v^C(x_{j-\frac{1}{2}}^+)\right] ,\end{aligned} \tag{49}$$

$$\int_{I_{j-\frac{1}{2}}} u_h^{n+1,D} \cdot v^D dx = \int_{I_{j-\frac{1}{2}}} u_h^{n+1,C} \cdot v^D dx \, , \tag{50}$$

In the reconstructed CDG method, (50) is used to replace (48) in the CDG method. The reconstructed CDG method is still high order as the CDG method and reduce the computational cost of the CDG method nearly half.

Reconstructed CDG method

Theorem

The numerical solution u_h^C and u_h^D of the RCDG method in (49)-(50) *with $F(u) = u$ satisfies the following L^2 stability condition*

$$\frac{1}{2}\frac{d}{dt}\int_a^b (u_h^C)^2 dx = -\frac{1}{\tau_{max}}\int_a^b \left(u_h^D - u_h^C\right)^2 dx + E \leq 0 \tag{51}$$

and

$$\int_a^b (u_h^D)^2 dx \leq \int_a^b (u_h^C)^2 dx \tag{52}$$

with a small CFL number, E is given by:

$$E = \sum_j \left(u_h^C(x_j, t) - \{u_h^D(x_j, t)\}\right) \lfloor u_h^D(x_j, t) \rfloor , \tag{53}$$

Herein $\{u_h^D(x_j, t)\} = \frac{1}{2}(u_h^D(x_j^+, t) + u_h^D(x_j^-, t))$ *and* $\lfloor u_h^D(x_j, t) \rfloor = u_h^D(x_j^-, t) - u_h^D(x_j^+, t)$.

Reconstructed CDG method

Theorem

The numerical solution u_h^C and u_h^D of the RCDG method in (49)-(50) *for $F(u) = u$ with a smooth initial condition $u(x,0) \in H^{k+1}$ satisfies the following L^2 error estimate*

$$\|u - u_h^C\|^2 \leq C(\Delta x)^{2k}, \|u - u_h^D\|^2 \leq C(\Delta x)^{2k}, \tag{54}$$

where u is the exact solution.

CDG method on unstructured overlapping meshes

We first define the unstructured overlapping meshes. The primal mesh (denoted by $\mathcal{T}^C$) is a triangulation of the computational domain Ω as in Figure (formed by the solid line). Then we take an interior point in each triangle and connect the point to the three vertices of the triangle by dashed line as in Figure, this forms the dual mesh (denoted by $\mathcal{T}^D$) which covers the primal mesh, and each edge on the primal mesh is located interior of an element on the dual mesh.

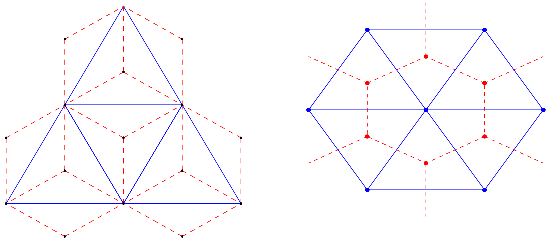

Figure: Unstructured overlapping meshes. Left: used in our work; right: used in Y. Liu's work. Solid line: primal mesh; dashed line: dual mesh.

CDG method on unstructured overlapping meshes

We consider the two-dimensional conservation laws:

$$\mathbf{U}_t + \nabla \cdot \mathbf{F}(\mathbf{U}) = 0, \tag{55}$$

The fully discretized CDG method for (55) is to look for $\mathbf{U}_h^{n+1,\star} \in \mathbf{W}_h^\star$ such that for any $\mathbf{V}^\star \in \mathbf{W}_h^\star|_{K^\star}$ with any $K^\star \in \mathcal{T}^\star$,

$$\begin{aligned}
\int_{K^C} \mathbf{U}_h^{n+1,C} \cdot \mathbf{V}^C dxdy &= \int_{K^C} \left(\theta_n \mathbf{U}_h^{n,D} + (1-\theta_n)\mathbf{U}_h^{n,C}\right) \cdot \mathbf{V}^C dxdy \\
&+ \Delta t_n \int_{K^C} \left[\mathbf{F}(\mathbf{U}_h^{n,D}) \cdot \nabla \mathbf{V}^C\right] dxdy \\
&- \Delta t_n \int_{\partial K^C} \left[\mathbf{F}(\mathbf{U}_h^{n,D}) \cdot \mathbf{n}_{K^C} \cdot \mathbf{V}^C\right] ds\,.
\end{aligned} \tag{56}$$

$$\begin{aligned}
\int_{K^D} \mathbf{U}_h^{n+1,D} \cdot \mathbf{V}^D dxdy &= \int_{K^D} \left(\theta_n \mathbf{U}_h^{n,C} + (1-\theta_n)\mathbf{U}_h^{n,D}\right) \cdot \mathbf{V}^D dxdy \\
&+ \Delta t_n \int_{K^D} \left[\mathbf{F}(\mathbf{U}_h^{n,C}) \cdot \nabla \mathbf{V}^D\right] dxdy \\
&- \Delta t_n \int_{\partial K^D} \left[\mathbf{F}(\mathbf{U}_h^{n,C}) \cdot \mathbf{n}_{K^D} \cdot \mathbf{V}^D\right] ds\,.
\end{aligned} \tag{57}$$

where $\mathbf{n}_{K^\star}$ denotes the outward unit normal vector of cell $K^\star$, $\theta_n = \Delta t_n/\tau \in [0,1]$ with τ being the maximal time step allowed by the CFL restriction.

CDG method on unstructured overlapping meshes

Theorem

The numerical solution U_h^C and U_h^D of the CDG method (56)-(57) with $F(U) = U$ satisfies the following L^2 stability condition

$$\frac{1}{2}\frac{d}{dt}\int_\Omega \left((U_h^C)^2 + (U_h^D)^2\right) dxdy = -\frac{1}{\tau_{max}}\int_\Omega \left(U_h^D - U_h^C\right)^2 dxdy \le 0 \qquad (58)$$

with compactly supported boundary condition.

Numerical results

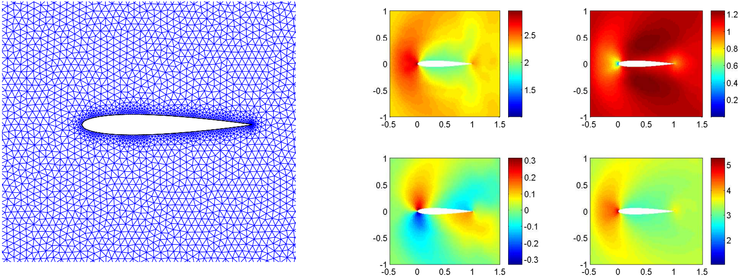

Figure: Left: Part of the primal mesh for the flow past an airfoil. Right: The contours of the numerical results at $t = 1$ for the flow past an airfoil(Top left: density; top right: velocity component u; bottom left: velocity component v; bottom right: pressure).

Thanks for your attention !